2024 IEEE/ASME International Conference on Advanced Intelligent Mechatronics (AIM)
July 15-19, 2024. Boston, MA, USA

Additively Manufactured Flexible Endoscope Driven By Guided Antagonistic Twisted String Actuation: A Pilot Experimental Evaluation

Edoardo Fratarcangeli, Andrea Govoni, Giuliano A. Giacoppo, Leonhard Heinrich, Roberto Meattini, Peter P. Pott and Gianluca Palli

***Abstract*—This paper provides a preliminary experimental assessment of a flexible endoscope driven by antagonistic twisted string actuation (TSA). Traditional endoscope designs have relied on manual manipulation or actuation systems lacking force control loops, limiting their versatility and ease of use. The proposed approach leverages the benefits of additive manufacturing to create customizable, deformable endoscope's tip structures, while TSA provides an efficient and potentially compact actuation mechanism. The experimental evaluation encompasses two key aspects of endoscope performance: tissue interaction and stiffness variation. Through a series of controlled experiments, the endoscope's ability to interact with mock biological tissues is assessed, demonstrating successful force application using both agonist-only and antagonistic functioning modalities. Furthermore, the endoscope's resilience to external disturbances is evaluated, with results showing significant improvements in stiffness and response to perturbations when utilizing antagonistic control. These findings highlight the potential of the proposed device to improve flexible endoscopy design and functionality. By integrating advanced manufacturing techniques with innovative actuation mechanisms, robotic flexible endoscopes can offer enhanced maneuverability, diagnostic precision, and patient safety.**

I. Introduction

Endoscopy is used by either doctors or surgeons to investigate symptoms in the digestive system, and perform biopsy-based diagnoses or cauterization. It is possible to subdivide into rigid and flexible endoscopy, on the basis of the specific application requirements [1]. In this work we focus on flexible endoscopes, since they enables improved minimally invasive diagnosis of pathologies. Conventional flexible endoscopes are actuated exploiting tendons, and include a distal component which can be bent by manually pulling the tendons through proper wheels available at the handle of the endoscope [2]. However, in recent decades advances in materials science and mechatronics have offered new avenues for improvements over conventional flexible endoscopes [3].

E. Fratarcangeli, A. Govoni, R. Meattini and G. Palli are with the Department of Electrical, Electronic, and Information Engineering (DEI), University of Bologna, 40136 Bologna, Italy.
G. A. Giacoppo, L. Heinrich, and P. P. Pott are with the Institute of Medical Device Technology, University of Stuttgart, 70569 Stuttgart, Germany.
This work was patially supported by DFG (INST 41/1123 FUGG), ERASMUS+, European Commission's Horizon Europe Framework Programme with the project IntelliMan under Grant 101070136 and MUR with the project "Sustainable Mobility Center" under Grant CN00000023-CUP J33C22001120001.

In the first place, the advent of additive manufacturing allows to conceive flexible endoscope tips constituted by *continuum* deformable structures made of polymeric material. This enables significant advantages in terms of smother interactions with biological soft tissues, dramatically reducing the risk of unintentional perforations [4], [5]. Second, the ease of availability of modern microcontroller and electric actuators allows to design flexible endoscopes in which the manual guidance is replaced by motorized drive units, typically rotational motors that pull tendons by means of proper pulleys. *De facto*, this scenario may open the door to the robotization of flexible endoscopy, with countless advantages. Operation reliability, motion repeatability, standardization of diagnosis procedures, even up to telemedicine scenarios [6]. In literature, robotic endoscopy systems have already been investigated. In [7], a flexible robot-assisted surgical system was proposed for total laryngectomy. A modular robotic system was presented by [8], whereas [9] equipped a standard colonoscope with teleoperable electric drives. However, a few primary issues still need to be addressed for the development of truly effective robotic flexible endoscopes. Endoscopes need to be equipped by force sensing, for a series of critical reasons. A force feedback at the actuation side is required in order to be able to compensate for undesired nonlinearities/nonidealities due to intrinsic tendon-based transmission elasticity and friction, and backlash [10]. Furthermore, it is fundamental to be able to apply desired force levels according to tissue characteristics and application purposes. Also, considering that space available in operating theaters is typically significantly limited, it is not conceivable to achieve robotization of flexible endoscopes at the cost of large and heavy systems, bulky to place and operate, as instead is the case of most of current proposed solutions [11]. Therefore, it is desirable to investigate actuation and system design solutions able to satisfy weight, size, transmission ratio and force sensing/control specifications to foster further advancement in the realization of effective robotic flexible endoscopes. Finally, minimization of encumbrance may take advantage from specific guiding of the tendons along non-straight paths from the motor to the endoscope bendable tip.

In this work, we report the results of a pilot experimental validation of a prototypal robotic flexible endoscope. Specifically, we present a 3D-printed endoscope tip driven by guided antagonistic Twisted String Actuation (TSA) [12]. TSA is a

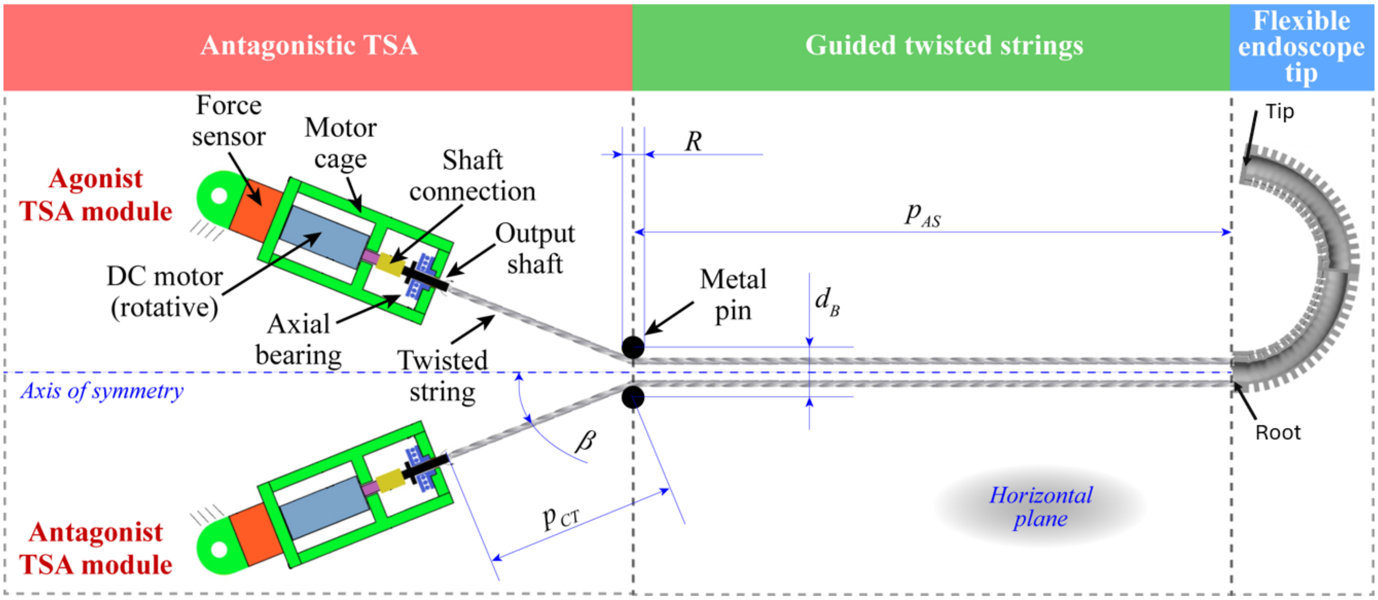

Fig. 1: Schematic representation of the antagonistically actuated flexible endoscope using two TSA modules (top view).

solution based on the conversion of a rotary motion into linear motion by the twisting of a string composed by two cables fixed each other at their extremities. The highly advantageous transmission ratio presented by the TSA mechanism [12] permits the usage of cheap, small and lightweight motors – typically simple DC motors – allowing to meet the desirable requirements of the actuation system. Integrated to the additively manufactured endoscope tip, two antagonistically operating TSA modules are exploited to achieve bidirectional motion for the application of different target forces and stiffness levels. In particular, a force sensor seamlessly integrated by design within the TSA modules is exploited for these purposes. The prototype was tested for its ability to interact with mock-up biological tissues. Using firstly an agonist-only actuation configuration, the endoscope was experimented for application of forces at varying tissue distances. Then, a second experiment leveraged the two antagonistic TSA modules to vary the endoscope stiffness to resist to external perturbations. The results successfully validate the prototypal system, highlighting its suitability for multiple requirements of force/stiffness modulation. The pilot study therefore provides positive outcomes for the realization of actual effective robotic flexible endoscopes by means of TSA-based actuation and additive manufacturing.

II. Materials and Methods

A. Overview Of The TSA-Based Flexible Endoscope

With reference to the schematic representation of the system reported in Fig. 1, the illustration of the proposed TSA-based flexible endoscope can be subdivided in the description of three subparts: the *antagonistic TSA*, *guided twisted strings*, and *flexible endoscope tip*.
The *antagonistic TSA* subpart includes two TSA modules, each of which composed by a DC motor, and a force sensor

TABLE I: System design parameters.

Description	*Variables*	*Values*
Guide angle	β	15°
Inclined twisted string length	p_{CT}	100 mm
Straight twisted string length	p_{AS}	900 mm
Metal pin's radius	R	2 mm
Distance Bolt	d_B	22 mm

able to measure axial forces. The TSA modules can control motion/force of the endoscope bendable tip by means of proper connection of the strings at both the module's output shaft and head of the endoscope: in such a way, the motor rotation transmits forces to the end-effector through the twisting of the strings. A detailed description of the TSA modules is provided in Sec. II-C. Furthermore, since in this work we wanted to investigate the exploitation of the TSA technology for reducing the overall bulkiness of the endoscopic system, we leveraged the flexibility of the strings to arrange the TSA modules with an inclination angle β on the horizontal plane with respect to the axis of symmetry of the system (see Fig. 1). In this way, the strings related to the two TSA modules were specularly aligned until reaching a desired distance between the agonist/antagonist strings, namely $d = d_B - 2R$, imposed by guiding the strings via two pins with radius R. Angle β was heuristically set equal to $15°$ as a working compromise to test a reduction of the overall length of the system while keeping a reasonably small portion of the string in contact with the metal pin, therefore limiting friction (eventually, this is in accordance with the well known Euler-Eytelwein equation, e.g. see [13]). System design parameters are reported in Table I (refer also to Fig. 1). The *guided twisted strings* subpart consists of the two strings related to the agonist/antagonist TSA modules aligned in parallel, in such way to build a straight path from the metal pins to the endoscope flexible tip. The length of the guided

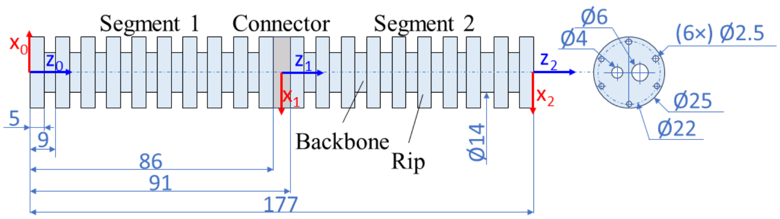

Fig. 2: The endoscope has two segments, each of which with a backbone with ribs. To accommodate the strings, ribs have six holes (unit measurement are mm). Two channels are present in the backbone for camera and instruments.

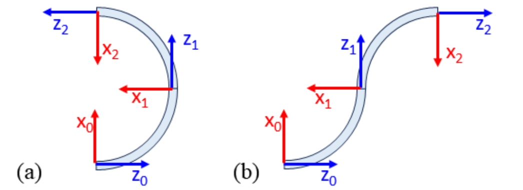

Fig. 3: Representation of two endoscope tip's segments in the x-y plane with (a) a deflection of 180° and (b) the formation of a sigmoid.

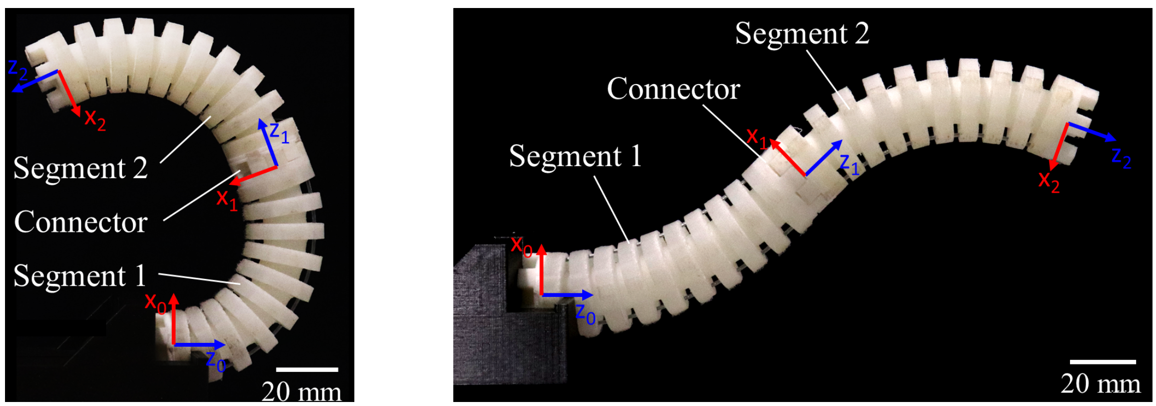

(a) Full deflection

(b) S-curve

Fig. 4: The additively manufactured endoscope tip (a) at full deflection and (b) forming an S-curve. The range of motions span by endoscope bending is approximately 100mm

twisted sting straight path p_{AS} (see Fig. 1 and Table I) was designed in order to have available an overall string length to ensure the necessary twisted string's contraction range for the actuation of the system (i.e. 20% of the full $p_{CT} + p_{AS}$ string length [12]). The *flexible endoscope tip* subpart is constituted by a flexible and continuous structure composed of multiple overlapping thermoplastic polyurethane (TPU) 3D-printed discs, resembling, to some extent, the conformation of a vertebral column. In this way, the endoscope tip was provided with the capability of bending by freely flexing/extending on the horizontal plane (see Fig. 1). A detailed description of the endoscope tip is provided in the subsequent Sec. II-B.

B. 3D-Printed Flexible Endoscope Tip

The endoscope flexible tip was designed as a monolithic, continuously flexible structure with a single backbone. With reference to Fig. 2, it consists of a tubular core (i.e., the backbone) connected to ten ribs made of TPU. Two central channels have been integrated into the backbone to allow the possibility of carrying instruments and camera. The design requirements are a uniform curvature of at least 180° and the creation of an S-shape by connecting the two segments of the flexure structure, with a rigid connector made of PolyCarbonate/Acrilonitrile-Butadiene-Stirene (PC-ABS) material, see Fig. 3. The tip was deflected by means of the strings, which passed through the specific holes present in the ribs, and then fitted with fixed nipples at their ends. Therefore, when actuated, the strings extremities were fixed axially in the direction of the linear force.

The endoscope tip was manufactured using a Freeformer 300-3X (Arburg GmbH & Co. KG, Lossburg, Germany). This 3D printer allowed the simultaneous processing of three different thermoplastics and works according to the droplet dispersion principle [14]. Similar to an injection moulding machine, plastic granules were melted in an extruder screw and then fed to the ejector unit. The droplets were formed by a high-frequency piezoelectric nozzle shutter positioned on the moving build platform in the heated build chamber. The segmented structure of the endoscope allowed production within the confines of the 3D printer's build envelope. The segment was printed vertically from the Desmopan 9385A (Covestro AG, Leverkusen, Germany). The connectors made of Bayblend FR3010 (Covestro AG) were seamlessly integrated into the printing process and located at the beginning and end of the segment. This integration ensured a direct connection between the connectors and the flexible segment. After printing, the water soluble carrier material Armat11 (Arburg GmbH & Co. KG) was washed off, allowing the two segments to be joined together to form the endoscope tip. The endoscope tip showed a total maximum deflection of 204°, which can be observed

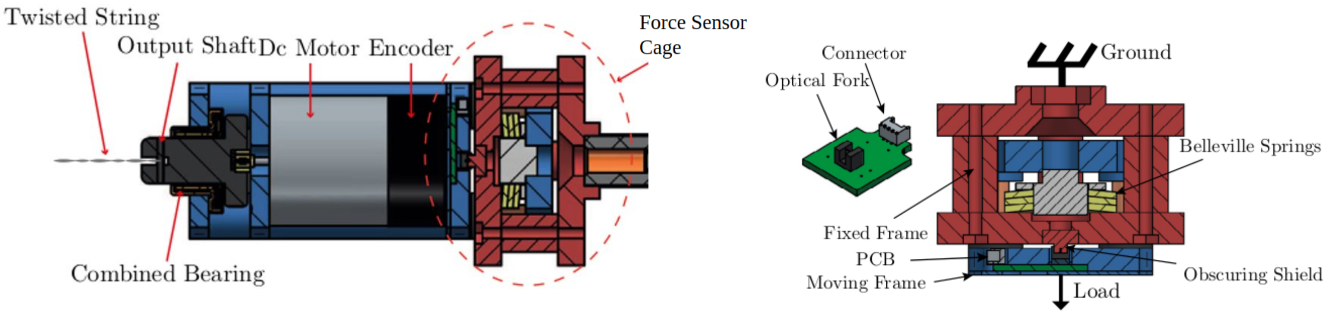

(a) Overall representation of the TSA module's components.

(b) Focus on the TSA module's force sensor.

Fig. 5: TSA module.

in the real endoscope tip reporeted Fig. 4a (required tensile force: 103 ± 5 N). Fig. 4b shows instead the reproduction of a sigmoid with a deflection of $45°$ for both proximal and distal endoscope tip segments.

C. TSA Module

In this section, we delve into the components of the TSA modules, providing an overview on the mechanical elements, along with control and sensor hardware. In terms of control hardware, we employed Arduino Nano, a cost-effective micro-controller utilized in this work for individualized motor control. Alongside, the H-bridge drive (L298N) was integrated. Each drive branch was managed by a single Arduino board, controlling an individual motor. Both motors were powered by L298N and received a supply of 12 V. Moving on to the mechanical and sensor hardware, the TSA module first of all included the strings to be twisted, which represent the actual mechanism transmission system, composed by two wires of Berkley WHIPLASH 8 braided polyethylene fiber, each of which with a diameter of 0.25 mm. A complete representation of the TSA module and its components can be observed in Fig. 5a. With reference to this figure, the module's motor-sensor block is constituted by the motor cage (in blue) and force sensor cage (in red). The motor cage comprised a DC motor, alongside a proper bearing and connection for the strings on the output shaft. This design solution ensured minimal torque perturbation, rigidly transferring motor's mechanical power to the module's output shaft. The twisting of the string could then occur thanks to the presence of a small metal peg mechanical interface to which the string was secured. In this way, the motor block was rigidly interconnected to the string and was subject to the axial forces acting from the twisted string. On the other hand, the force sensor cage, as illustrated in Fig. 5b, incorporated Belleville springs arranged in series and the force sensor PCB, the latter comprising an optical fork featuring a phototransistor (KRB011) and an OpAmp (MCP6001T-I/OT). This solution was capable of measuring axial forces applied to the TSA module, exploiting a consequent displacement between an obscuring shield and the PCB. Indeed, a small relative movement between the motor cage and the force sensor block, due to linear forces acting on the twisted string, generates a displacement of the obscuring shield that activates the phototransistor. Then, the Belleville springs, which was securely positioned and linked to both the moving and fixed blocks, retract the moving block when the force from the twisted string ceases, thus restoring the motor cage.

D. TSA Modules And Endoscope Control

The control of each TSA module of the endoscope presented in this work was realized by a standard PID controller, which was encoded in the Arduino Nano board (see Sec. II-C) to deliver corresponding control inputs to the DC motor. The system operated by the setting of a force reference F_{ref}, which the controller tracked through DC motor's voltage PWM modulation, i.e. outputting a PWM's duty cycle $d_C(t)$ by taking as input a tracking error $e_F(t)$ computed as

$$e_F(t) = F_{\text{ref}} - F_S(t), \tag{1}$$

where $F_S(t)$ is the force measured by the TSA module's force sensor. Eventually, note that positive/negative rotation direction of the DC motor was determined on the basis of the sign of $e_F(t)$ as given in eq. (1), and enforced through the H-bridge in order to reverse the motor's voltage polarity. Eventually, note the Arduino board provided all the digital and analog interfaces necessary for data exchange with TSA module control hardware components, as well as the acquisition of the force sensor signal and the connection to the power supply. Therefore, exploiting the PID force control for each single TSA module just introduced, two different working modalities were implemented for the flexible endoscope presented in this study, the *agonist-only functioning* and the *antagonistic functioning*, as detailed in the following.

1) Agonist-only functioning: In this working modality, a desired reference force F_{des} was imposed in eq. (1) (i.e. $F_{\text{ref}} := F_{\text{des}}$) only for a single TSA module of the endoscope, either to one or the other, which therefore acted as the "agonist-only" actuator for the bending of the flexible tip. Differently, for the remaining TSA module, the reference force was invariably set as equal to zero. Therefore, this TSA module was just idle, favoring the bending of the endoscope tip as imposed by

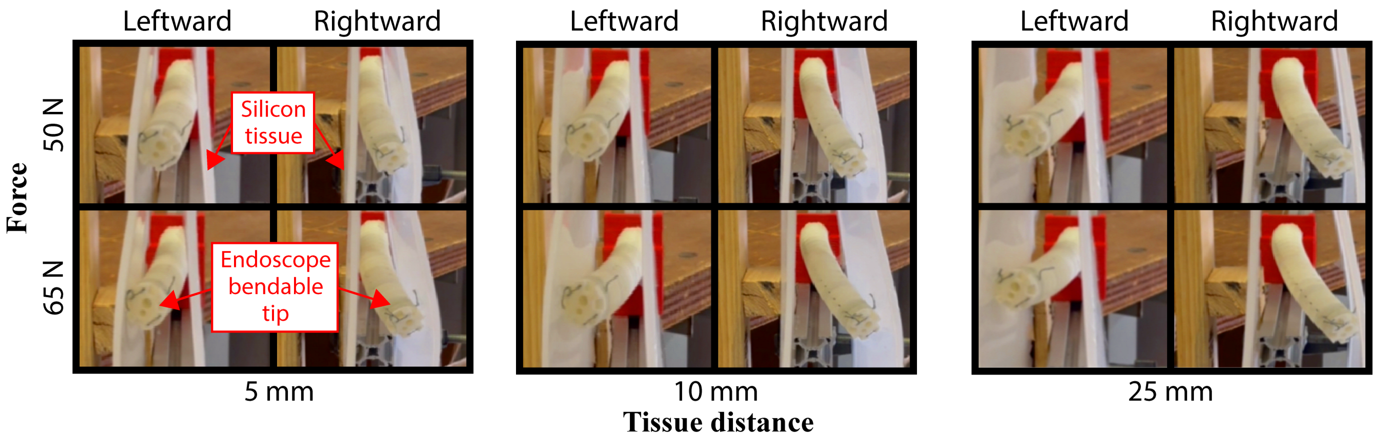

Fig. 6: Shots from the tissue interaction experimental validation, for the different combinations of reference force, tissue distance and endoscope tip bending direction.

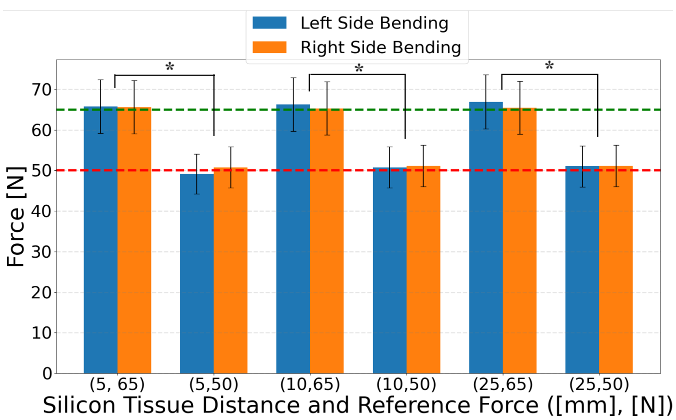

Fig. 7: Results of the tissue interaction experimental validation. Bars and whiskers indicate mean value and standard deviations, respectively. Symbol "*" indicates statistical significant difference, $p < .05$

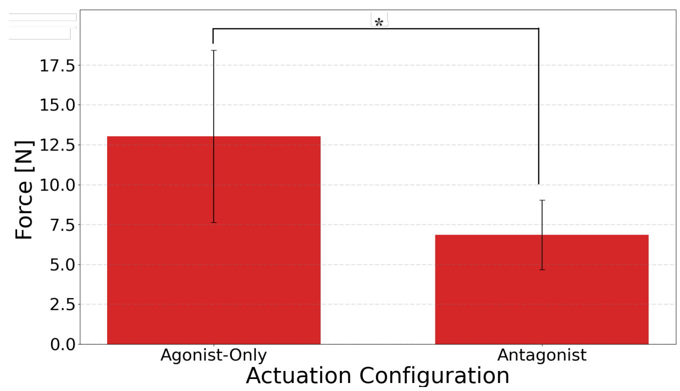

Fig. 8: Results of the stiffness increase experimental validation. Bars and whiskers indicate mean value and standard deviations, respectively. Symbol "*" indicates statistical significant difference, $p < .05$.

the agonist-only actuator. Note that no possibility of stiffness control was possible in this modality, and the endoscope could resist forces only in the flexing direction of the tip bending.

2) Antagonistic functioning: In this modality, a force reference was provided to both TSA modules, that is, they were both active. For the antagonist TSA module, a reference force $F_{\text{ref}} := F_{\text{des}}^{\text{antagonist}}$ was imposed, whereas for the agonist TSA module a reference force $F_{\text{ref}} := F_{\text{des}}^{\text{antagonist}} + F_{\text{des}}^{\text{agonist}}$. $F_{\text{des}}^{\text{antagonist}}$ and $F_{\text{des}}^{\text{agonist}}$ are the desired forces for the antagonist and agonist actuators, respectively. Therefore, in this way it was possible to both control the force of the agonist actuator and the stiffness of the bendable tip, as well as resist forces in both flexing and extending directions as much as the endoscope stiffness is increased.

III. Pilot Experimental Validation And Results

A. Tissue Interaction Experimental Validation

1) Experiment Description: The aim of this experiment was to test actions performed on biological tissue during a medical procedure. Specifically, within the preliminary validations carried out in this study, we focused on assessing the endoscope's ability to interact with a mock-up biological tissue realized by using silicon (see Fig. 6). The experiment involved validating the capability of the proposed endoscope to apply a constant force to the tissue using the agonist-only functioning modality described in Sec, II-D1. In the experiment, three different distances of the tissue from the endoscope bendable tip were tested. Fig. 6 illustrates the tests with a tissue distance of 5 mm, 10 mm and 25 mm, with bending of the tip in both leftward and rightward directions. Two different reference force levels were tested: 50 N and 65 N. For each triplet of experimental conditions (i.e.: tissue distance, bending direction, force reference level), the test was repeated 10 times, and force sensor measurements were collected.

2) Results Of The Validation: The experiment demonstrated that, for every test configuration, the TSA modules were capable to apply the desired reference force, resulting in the associated bending of the endoscope tip and interaction with the tissue. Fig. 7 reports the bar graph of the mean value over the test repetitions of forces measured for each combination of tissue distances and reference force levels, showing as the TSA modules of the endoscope successfully reached the required force. Furthermore, the statistical test *t-test* was performed to verify if the difference between the boxplots is statistically significant or not. Measured forces revealed to be statistically significantly different for distinct reference force levels —- $t(18) = 11.5$, $t(18) = 11.3$ and $t(18) = 10.2$ for 5 mm, 10 mm and 25 mm tissue distance, repsectively, $p < .05$.

B. Stiffness Increase Experimental Validation

1) Experiment Description: The experiment aimed to validate the effectiveness of the antagonistic functioning modality illustrated in Sec. II-D2. To this purpose, a comparison test was carried out, using the same setup as depicted in Figure 6, with controlled perturbations applied to the distal end of the endoscope. First, the endoscope tip was bent at a constant angle of approximately 20^o by means of the agonist-only functioning modality (Sec, II-D1), and 10 impulsive force perturbations of the amplitude of 5 N were applied in the direction of the tip flexion. Thereafter, in a second test the antagonistic functioning modality (Sec. II-D2) was tested against the same 10 force perturbations. Data from the force sensors was collected during the test.

2) Results Of The Validation: Fig. 8 clearly illustrates the different behaviors of the two considered endoscope functioning modalities, evaluated on the basis of the collected sensor values. The bar graph depicts the mean of repeated agonist TSA module's force undershoots resulting from external impulsive disturbances (as described in the previous subsection), in both the agonist-only and antagonistic testing conditions. The antagonistic working modality exhibited a statistically significantly lower mean value of the force undershoots with respect to the agonist-only modality ($t(18) = 6.1$, $p < .05$). This was due to the more effective counteractive action against external perturbations provided in the flexion direction of the endoscope bendable tip, thanks to the possibility of enforcing a higher stiffness level.

IV. Conclusions

In this paper, we introduced a novel prototype robotic flexible endoscope by integrating guided antagonistic TSA with an additively manufactured bendable tip. Through pilot experimental evaluations, we validated the endoscope's ability to interact with biological tissues and resist external disturbances. The results demonstrated successful force application and tissue interaction using agonist-only control, with further enhancements in stiffness and resilience achieved through antagonistic control. These findings highlight the potential of the TSA-based transmission system and additive manufacturing for realizing effective robotic flexible endoscopes, with positive perspective for future developments in the direction of endoscopes with truly improved maneuverability and diagnostic capabilities. Future research will focus on several short, medium and longer term works, including: optimizing the setup's structure, reducing the size of endoscope parts, utilizing motor encoders for improved control, and potentially adding more TSA modules to expand motion capabilities.

References

[1] K. Schwab and S. Singh, "An introduction to flexible endoscopy," *Surgery (Oxford)*, vol. 29, no. 2, pp. 80–84, 2011.

[2] D. Schlesiger, G. A. Giacoppo, M. B. Schäfer, and P. P. Pott, "Twisted string actuation with position feedback for robotic endoscopy," *Current Directions in Biomedical Engineering*, vol. 7, no. 2, pp. 343–346, 2021.

[3] B. Seeliger and L. L. Swanström, "Robotics in flexible endoscopy: current status and future prospects," *Current opinion in gastroenterology*, vol. 36, no. 5, pp. 370–378, 2020.

[4] Y. Shapiro, A. Wolf, and G. Kósa, "Compliant bi-bellows actuator with pvdf force-shape sensing," in *2012 4th IEEE RAS & EMBS International Conference on Biomedical Robotics and Biomechatronics (BioRob)*. IEEE, 2012, pp. 1602–1606.

[5] G. Stano, L. Arleo, and G. Percoco, "Additive manufacturing for soft robotics: Design and fabrication of airtight, monolithic bending pneunets with embedded air connectors," *Micromachines*, vol. 11, no. 5, p. 485, 2020.

[6] L. Manfredi, *Endorobotics: Design, R&D and Future Trends*. Academic Press, 2022.

[7] P. J. Schuler, T. K. Hoffmann, J. A. Veit, N. Rotter, D. T. Friedrich, J. Greve, and M. O. Scheithauer, "Hybrid procedure for total laryngectomy with a flexible robot-assisted surgical system," *The International Journal of Medical Robotics and Computer Assisted Surgery*, vol. 13, no. 2, p. e1749, 2017.

[8] S. J. Phee, S. C. Low, V. Huynh, A. P. Kencana, Z. Sun, and K. Yang, "Master and slave transluminal endoscopic robot (master) for natural orifice transluminal endoscopic surgery," in *2009 Annual International Conference of the IEEE Engineering in Medicine and Biology Society*. IEEE, 2009, pp. 1192–1195.

[9] D. J. Abbott, C. Becke, R. I. Rothstein, and W. J. Peine, "Design of an endoluminal notes robotic system," in *2007 IEEE/RSJ International Conference on Intelligent Robots and Systems*. IEEE, 2007, pp. 410–416.

[10] Y. Chen, J. M. Oliveira, and I. W. Hunter, "Sensor architecture for a two-actuator robotic endoscope tip," in *2011 Annual International Conference of the IEEE Engineering in Medicine and Biology Society*. IEEE, 2011, pp. 8340–8343.

[11] J. Kim, M. de Mathelin, K. Ikuta, and D.-S. Kwon, "Advancement of flexible robot technologies for endoluminal surgeries," *Proceedings of the IEEE*, vol. 110, no. 7, pp. 909–931, 2022.

[12] G. Palli, C. Natale, C. May, C. Melchiorri, and T. Wurtz, "Modeling and control of the twisted string actuation system," *IEEE/ASME Transactions on Mechatronics*, vol. 18, no. 2, pp. 664–673, 2012.

[13] R. A. Becker, "Introduction to theoretical mechanics," 1954.

[14] D. Von Zeppelin and M. Manka, "Arburg plastic freeforming," *Engineering of Biomaterials*, vol. 20, 2017.